University of Dayton
eCommons

Electrical and Computer Engineering Faculty Publications

Department of Electrical and Computer Engineering

4-2011

Binary and Core-Shell Nanoparticle Dispersed Liquid Crystal Cells for Metamaterial Applications

George Nehmetallah
The Catholic University of America

Rola Aylo
The Catholic University of America

Partha P. Banerjee
University of Dayton, pbanerjee1@udayton.edu

Follow this and additional works at: http://ecommons.udayton.edu/ece_fac_pub


Part of the Computer Engineering Commons, Electrical and Electronics Commons, Electromagnetics and Photonics Commons, Optics Commons, Other Electrical and Computer Engineering Commons, and the Systems and Communications Commons

eCommons Citation

Nehmetallah, George; Aylo, Rola; and Banerjee, Partha P., "Binary and Core-Shell Nanoparticle Dispersed Liquid Crystal Cells for Metamaterial Applications" (2011). *Electrical and Computer Engineering Faculty Publications.* Paper 105.
http://ecommons.udayton.edu/ece_fac_pub/105

This Article is brought to you for free and open access by the Department of Electrical and Computer Engineering at eCommons. It has been accepted for inclusion in Electrical and Computer Engineering Faculty Publications by an authorized administrator of eCommons. For more information, please contact frice1@udayton.edu, mschlangen1@udayton.edu.

Journal of Nanophotonics

SPIEDigitalLibrary.org/jnp

Binary and core-shell nanoparticle dispersed liquid crystal cells for metamaterial applications

Georges Nehmetallah
Rola Aylo
Partha P. Banerjee

SPIE

Binary and core-shell nanoparticle dispersed liquid crystal cells for metamaterial applications

Georges Nehmetallah, Rola Aylo, and Partha P. Banerjee
University of Dayton, Department of Electrical and Computer Engineering and Electro-Optics Program, 300 College Park, Dayton, Ohio 45469

Abstract. We theoretically explored the feasibility of a tunable metamaterial using binary as well as core-shell nanoparticle dispersed liquid crystal cells in the infrared and optical regimes. Owing to the spatial variation of the permittivity of the liquid crystal host upon the application of a bias voltage, the host was decomposed into a layered medium and the effective refractive index recalculated for each layer due to the distribution of polaritonic and plasmonic nanoparticles. The scattering, extinction, and absorption of such a nanoparticle dispersed liquid crystal cell were also found. Depending on the applied voltage bias across the liquid crystal host, the types of nanoparticles used, and their radii and volume-filling fractions in the liquid crystal host, near-zero as well as negative index of refraction can be obtained over a range of frequencies, according to the effective medium theory. *© 2011 Society of Photo-Optical Instrumentation Engineers (SPIE)*. [DOI: 10.1117/1.3576117]

Keywords: metamaterials; nanoparticles; liquid crystal; negative index; effective medium theory.

Paper 10093SSPR received Dec. 9, 2010; revised manuscript received Feb. 8, 2011; accepted for publication Mar. 17, 2011; published online Apr. 26, 2011.

1 Introduction

During the last decade, and after Pendry's famous paper on superresolution using a superlens,[1] there has been a plethora of work on metamaterials. Metamaterials are artificial materials that exhibit strong magnetic and electric response in a certain range of frequencies that may result in a negative refractive index which leads to new optical phenomena such as negative refraction,[2] superlensing,[1] and can lead to numerous possible applications such as sensors[3] and cloaking.[4] A lot of work has been dedicated to make such a metamaterial practical, low cost, and tunable. Using a tunable material such as liquid crystal (LC) to construct such a structure has been reported in the literature by the group of Khoo et al.[5–9] In their work they have used core-shell nanospheres to theoretically demonstrate negative index materials (NIMs) in the terahertz regime.[5] Also, they have recently used a dye doped nematic liquid crystal showing a lowered loss in the UV region of the spectrum where the real part of the index of refraction is less than unity but not negative.[8]

LCs have large optical anisotropy and are sensitive to temperature and external electromagnetic fields which make them good candidates for dynamic metamaterials.[10,11] Since nematic LCs are anisotropic materials, the physical properties of the system vary with the average alignment profile of the director. Nematic LCs are characterized by an orientational order but not a translational order. The principal axes of the molecules are oriented on an average along a direction called the director which is apolar in nature. In the smectic phase, in addition to the orientational order, a one dimensional translational order is also present, resulting in a layered arrangement of the LC molecules.

The most important advantages of this approach are: a. ease of obtaining/designing NIMs in the IR/optical range, b. tunability depending on the electric (and possibly, magnetic or optical)

1934-2608/2011/$25.00 © 2011 SPIE

fields applied to the LC cell (LCC), volume filling fraction, nanoparticle size, etc., c. ease of fabrication, and d. low cost. Finally, one can incorporate a large variety of nanoparticles due to the fluid nature of LC.

Our work is mainly based on binary nanoparticles dispersed in a nematic LC for both the IR and optical regimes, while the work reported in Refs. 5–8 uses core-shell nanoparticles. The binary nanoparticles used for IR in our calculations are similar to those used for core-shell structures in Refs. 5–8. The nanoparticles used in our optical regime calculations, viz., Ag and CuCl (for both binary and core-shell cases), which use the excitonic property of the polaritonic materials, are different from those in Refs. 5–8. Furthermore, while it is true that we have used the same host, viz., nematic LCs as suggested in Refs. 5–9, we take into account the spatial variation in the permittivity, or equivalently the refractive index, of the LC host when a bias voltage is applied to the nanoparticle dispersed LC cell (NDLCC) structure. As is well-known, the spatial variation arises due to the fact that the molecular reorientation profile upon application of a bias voltage spatially modulates the permittivity (and hence the refractive index) of the LC, assumed to be nematic in this paper. Hence in our analysis, the host is treated as a layered medium with each layer possessing a different index of refraction due to the bias voltage, and thereafter, the effective refractive index profile due to the presence of nanoparticles of the layered structure is calculated using effective medium theory. So, in the biased case, the profile of the director angle and hence the refractive index (or permittivity) is numerically computed using COMSOL by simultaneously solving the Euler–Lagrange equation and the relation between the voltage and the director angle. This profile is thereafter discretized by decomposing the LCC into multilayers, and the effective refractive index in each layer is computed using effective medium theory.

The paper is organized as follows. In Sec. 2, a summary of the effective medium theory using Maxwell Garnett (MG) is presented, and applied to the case of binary and core-shell nanoparticles in a LC host. In Sec. 3 we present illustrative numerical results based on effective medium theory for NDLCCs made from various binary and core-shell nanoparticles. In particular, we examine the effective refractive index based on the angle between the propagation vector and the director axis, the effective real and imaginary parts of the refractive index through the biased NDLCC structure, and the effect(s) of changing the sizes of the nanoparticles and their filling fractions with a view to determine the tunability of the device. Section 4 concludes the paper.

2 Analysis of NDLCCs Using Effective Medium Theory

Pertinent IR/optical materials used for NDLCCs are characterized by their relative permittivity $\varepsilon = \varepsilon' + i\varepsilon''$ and relative permeability $\mu = \mu' + i\mu$. We start by using the Maxwell–Garnet formula and the Mie scattering theory applied to NDLCCs. Two cases are considered: a. binary dispersed nanoparticles and b. core-shell dispersed nanoparticles.

Consider the case of binary dispersed nanoparticle scatterers of permittivities $\varepsilon_1, \varepsilon_2$ and permeabilities μ_1, μ_2, respectively, in a host medium of permittivity ε_3 and permeability μ_3, as shown in Fig. 1. In order to formulate the equations that govern the electromagnetic (EM) material properties of NDLCCs, we adopt the MG mixing theory.[12–14] In the NDLCCs, we have a medium with three different regions: the LC host material (region 3), the "polaritonic" nanoparticles (region 1), and the plasmonic nanoparticles (region 2). Since all materials are assumed to be nonmagnetic, their relative permeabilities can be set to be equal to 1.

Good candidates for polaritonic nanoparticle materials are a. $LiTaO_3$ in the far IR (FIR) regime ($\approx 10^{12}$ Hz),[15] b. TlBr, TlCl, SiC in the mid-IR regime ($\approx 10^{13}$ Hz),[16] and c. Cu_2O, CuCl in the optical regime ($\approx 10^{14}$ Hz).[17] Their permittivities vary according to the Drude–Lorentz model and can be expressed as, for instance,

$$\varepsilon_1 = \varepsilon_\infty \left(1 + \frac{\omega_L^2 - \omega_T^2}{\omega_T^2 - \omega^2 - i\omega\gamma_1}\right) \qquad \text{(FIR)}, \tag{1a}$$

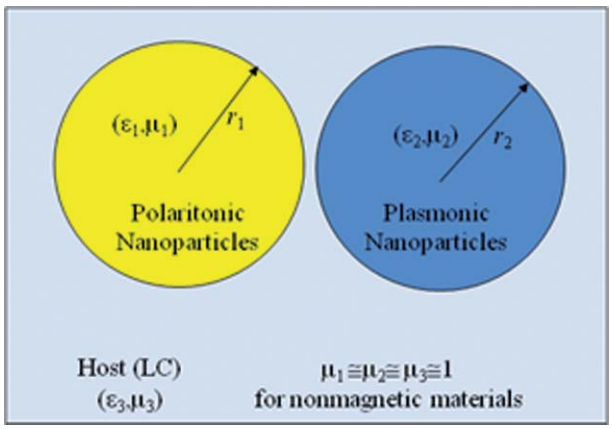

Fig. 1 Schematic of the metamaterials comprising binary nanoparticles distributed in nematic LC.

$$\varepsilon_1 = \varepsilon_\infty + A\frac{\gamma_1}{\omega_0 - \omega - i\gamma_1} \qquad \text{(optical)}, \tag{1b}$$

where $\omega_L = \omega_T\sqrt{\varepsilon_0/\varepsilon_\infty}$ (Sachs–Teller relation), ε_0 is the static dielectric constant, ε_∞ is the high frequency limit of the permittivity, ω_T and ω_L are the transverse and longitudinal optical phonon frequencies, respectively, γ_1 is the damping coefficient, the constant A is proportional to the exciton oscillation strength, and ω_0 is the exciton–polariton resonance frequency.

Good candidates for plasmonic nanoparticle materials are Ge, Ag, Au, and Cu, where their permittivities vary according to the Drude model:

$$\varepsilon_2 = \varepsilon_0\left(1 - \frac{\omega_p^2}{\omega^2 + i\omega\gamma_2}\right), \tag{2}$$

where ω_p is the plasma frequency (proportional to the square root of the impurity density for a semiconductor), and γ_2 is the damping factor similar to γ_1 defined above.[18]

Finally, for the LC host and for linearly extraordinary polarized light, the permittivity is given by[5,7,8,19]

$$\varepsilon_3 = \frac{\varepsilon_\parallel \varepsilon_\perp}{\varepsilon_\parallel \cos^2\theta + \varepsilon_\perp \sin^2\theta}, \tag{3}$$

where $\varepsilon_\parallel$ and $\varepsilon_\perp$ are the permittivities for light polarized parallel and perpendicular to the director axis $\hat{n}$, respectively, and θ is the angle between the director axis and the optical wave vector $\boldsymbol{k}$ of the incident wave.

As stated in Sec. 1, it is important to note that while for an unbiased LCC, the angle between the $\boldsymbol{k}$ vector of the light and the director axis is constant as shown in Fig. 2(a), for a biased LCC [as shown in Fig. 2(b)], the permittivity (or equivalently, the refractive index), is not constant throughout the LCC, but varies according to the profile sketched in Fig. 2(c) or 2(d). Hence, in the analysis of the NDLCC, we need to consider the biased LCC as a layered structure, each with its own permittivity or refractive index, and containing a distribution of binary (or core-shell) nanoparticles.

The effective permittivity ε_{eff} and the effective permeability μ_{eff} of the NDLCC can be found according to the *extended* MG theory (EMG), which is like the regular MG theory but

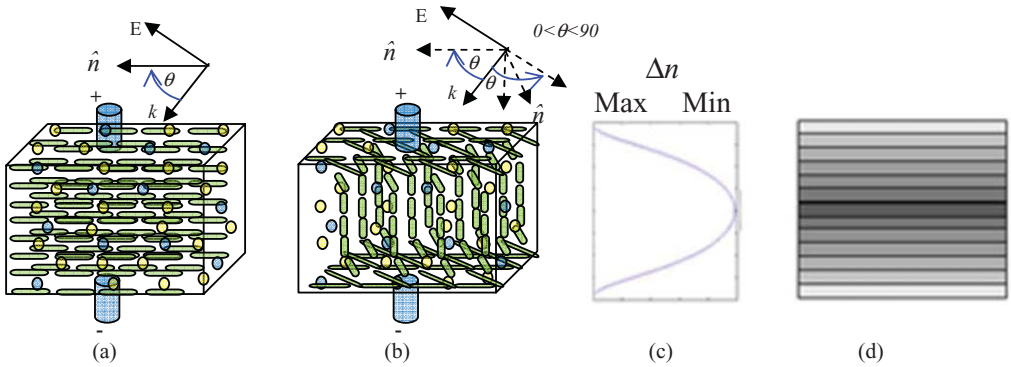

Fig. 2 (a) Artist's representation of director axis profile with no electric field applied to the NDLCC. θ represents the angle between the ***k*** vector of the light and the director axis, and (b) artist's representation of director axis profile with electric field applied to the LCC. The θ's denote representative angles between the ***k*** vector of the light and the various director axes at any location along the thickness of the NDLCC, (c) artist's representation of the change of index profile of the host LC due to the electric field (bias), (d) equivalent setup showing a layered stack with each layer's index of refraction according to the profile in (c). In the NDLCC, each layer's refractive index is further modified due to presence of nanoparticles.

with the incorporation of Mie scattering theory.[13–15] These relations are given by:

$$\varepsilon_{(1,2)}^{\text{eff}} = \varepsilon_3 \left(\frac{x_{3(1,2)}^3 - i3 f_{(1,2)} T_{1(1,2)}^E}{x_{3(1,2)}^3 + i(3/2) f_{(1,2)} T_{1(1,2)}^E} \right), \quad \mu_{(1,2)}^{\text{eff}} = \mu_3 \left(\frac{x_{3(1,2)}^3 - i3 f_{(1,2)} T_{1(1,2)}^H}{x_{3(1,2)}^3 + i(3/2) f_{(1,2)} T_{1(1,2)}^H} \right), \tag{4}$$

where $x_{3(1,2)} = k_3 r_{1,2} = \sqrt{\varepsilon_3 \mu_3}\omega r_{1,2}/c$, $x_{1,2} = \sqrt{\varepsilon_{1,2}\mu_{1,2}}\omega r_{1,2}/c$ stand for the sphere size parameters in the host and the sphere mediums, respectively, $r_{1,2}$ are the physical radii of the polaritonic and plasmonic spheres, respectively, and $f_{(1,2)} = 4\pi N r_{1,2}^3/3$ is the volume filling fraction occupied in the host by the scatterers. Also in Eq. (4),

$$T_{n(1,2)}^{E[H]}(\omega) = \frac{j_n(x_{(1,2)})[\psi_n(x_{3(1,2)})]'\varepsilon[\mu]_{(1,2)} - j_n(x_{3(1,2)})[\psi_n(x_{(1,2)})]'\varepsilon[\mu]_3}{h_n^{(1)}(x_{3(1,2)})[\psi_n(x_{(1,2)})]'\varepsilon[\mu]_3 - j_n(x_{(1,2)})[\xi_n(x_{3(1,2)})]'\varepsilon[\mu]_{(1,2)}}, \tag{5}$$

are the n'th order electric-dipole (magnetic-dipole) components of the scattering T matrix of a single sphere, $j_n(z) = \sqrt{\pi/2z} J_{n+0.5}(z)$, $y_n(z) = \sqrt{\pi/2z} Y_{n+0.5}(z)$, where J_n, Y_n are the n'th order spherical Bessel (Bessel) functions of the first and second types, respectively, and $h_n^{(1)}(z) = j_n(z) + i y_n(z)$ is the n'th order spherical Hankel function of the first type. Also the functions $\psi_n(z) = z j_n(z) = \sqrt{\pi z/2} J_{n+0.5}(z)$, $\chi_n(z) = -z y_n(z) = -\sqrt{\pi z/2} Y_{n+0.5}(z)$ are called the n'th order Riccati–Bessel functions of first and second type, respectively, and $\xi_n(z) = z h_n^{(1)}(z) = \sqrt{\pi z/2} H_{n+0.5}^{(1)}(z) = \psi_n(z) - i\chi_n(z)$ is the n'th order Riccati–Hankel function of first type, with

$$\psi_n'(z) = \frac{1}{2}\sqrt{\frac{\pi}{2z}} J_{n+0.5}(z) + \frac{1}{2}\sqrt{\frac{\pi z}{2}} \left[J_{n-0.5}(z) - J_{n+1.5}(z) \right], \tag{6a}$$

$$\chi_n'(z) = -\frac{1}{2}\sqrt{\frac{\pi}{2z}} Y_{n+0.5}(z) + \frac{1}{2}\sqrt{\frac{\pi z}{2}} \left[Y_{n-0.5}(z) - Y_{n+1.5}(z) \right]. \tag{6b}$$

From Eq. (5), the scattering, extinction, and absorption coefficients are given by:

$$Q_{sca,i} = \frac{2}{x_{3i}} \sum_{n=1}^{\infty} (2n+1)\left(\left|T_{ni}^{E}\right|^2 + \left|T_{ni}^{H}\right|^2\right), \tag{7a}$$

$$Q_{ext,i} = -\frac{2}{x_{3i}} \sum_{n=1}^{\infty} (2n+1)\,\mathrm{Re}\left(T_{ni}^{E} + T_{ni}^{H}\right), \tag{7b}$$

$$Q_{abs,i} = Q_{ext,i} - Q_{sca,i}. \tag{7c}$$

Thus, the scattering cross section exhibits several resonances depending on the radii of the nanoparticles, and the scattering is very efficient at these wavelengths. For absorptive materials, the intensity of light beam decreases as $\propto e^{-\alpha_i l}$ over a cell of thickness l, where $\alpha_i = (\pi r_i^2/a^3)(Q_{\mathrm{abs},i} + Q_{\mathrm{sca},i}) = \pi r_i^2 Q_{\mathrm{ext},i}$.

For the above equations to be valid, the quasistatic limit of the MG mixing rule, also known as EMG formula, obtained from Mie scattering theory need to be used. Note that the condition $x_{3(1,2)} = k_3 r_{1,2} \ll 1$ must be satisfied; although it is not necessary that $x_{1,2} \ll 1$. Unlike the static limit, the effective medium parameters in the quasistatic limit are dispersive even for a medium composed of nondispersive components. The EMG method can be used to calculate all the optical properties of the composite medium. In particular, the effective index $n_{\mathrm{eff}} = \sqrt{\varepsilon_{\mathrm{eff}}\mu_{\mathrm{eff}}}$ can be used in the Snell's law to find the refraction of the incident beam. Note that the EMG effective constants obtained are complex even in the case of nonabsorbing spheres embedded in a nonabsorbing host. In this case the imaginary part is due to the extinction of the propagating beam due to scattering. Thus, EMG cannot be used to find absorption.

For a binary composite comprising two different kinds of nanospheres, the effective medium parameters can be obtained from the condition that the average extinction of random unit cells compared with that of the surrounding medium is zero[15] and the effective permittivity and permeability for the 1st order $n = 1$ are expressible through the relations

$$C_1 \frac{\varepsilon_3 - \varepsilon_{\mathrm{eff}} - 3i/(2x_{3(1)}^3)T_{1,1}^{E} f_{12}(2\varepsilon_3 + \varepsilon_{\mathrm{eff}})}{\varepsilon_3 + 2\varepsilon_{\mathrm{eff}} - 3i/\left(x_{3(1)}^3\right)T_{1,1}^{E} f_{12}(\varepsilon_3 - \varepsilon_{\mathrm{eff}})} + C_2 \frac{\varepsilon_3 - \varepsilon_{\mathrm{eff}} - 3i/\left(2x_{3(2)}^3\right)T_{1,2}^{E} f_{12}(2\varepsilon_3 + \varepsilon_{\mathrm{eff}})}{\varepsilon_3 + 2\varepsilon_{\mathrm{eff}} - 3i/(x_{3(2)}^3)T_{1,2}^{E} f_{12}(\varepsilon_3 - \varepsilon_{\mathrm{eff}})} = 0, \tag{8a}$$

$$C_1 \frac{\mu_3 - \mu_{\mathrm{eff}} - 3i/(2x_{3(1)}^3)T_{1,1}^{H} f_{12}(2\mu_3 + \mu_{\mathrm{eff}})}{\mu_3 + 2\mu_{\mathrm{eff}} - 3i/(x_{3(1)}^3)T_{1,1}^{H} f_{12}(\mu_3 - \mu_{\mathrm{eff}})} + C_2 \frac{\mu_3 - \mu_{\mathrm{eff}} - 3i/(2x_{3(2)}^3)T_{1,2}^{H} f_{12}(2\mu_3 + \mu_{\mathrm{eff}})}{\mu_3 + 2\mu_{\mathrm{eff}} - 3i/(x_{3(2)}^3)T_{1,2}^{H} f_{12}(\mu_3 - \mu_{\mathrm{eff}})} = 0, \tag{8b}$$

where $f_{12} = f_1 + f_2$ is the total filling fraction of the spheres, $C_1 = f_1/f_{12}$, $C_2 = f_2/f_{12}$ are the relative concentrations of the spheres types 1 and 2, respectively. An estimate of the maximum filling factors f of the nanoparticles can be obtained by assuming certain lattice structures. For

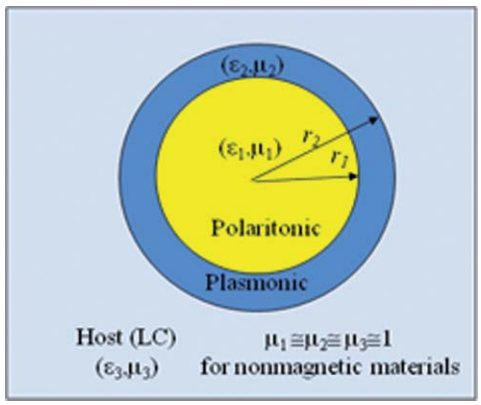

Fig. 3 Schematic of the metamaterials comprising core-shell nanoparticles randomly distributed in aligned nematic LC.

instance,

$$f = \begin{cases} 74\% : \text{fcc lattice}, \\ 34\% : \text{diamond lattice}. \end{cases} \tag{9}$$

For the case of core-shell nanoparticles shown in Fig. 3, we can adopt the same MG mixing rule described above. In this case, we again have a medium with three different regions: the LC host material (region 3), the shell (region 2), and the core (region 1). Since all three materials are nonmagnetic, their relative permeabilities can again be set equal to 1. At or near resonance, the combination of the effective permittivities with that of the field-induced permittivity change in the NDLCCs host results in this effective refractive index to vary from positive to near-zero/negative refraction phenomenon. Good candidates for polaritonic and plasmonic nanoparticles have been discussed above.

In the core-shell case, the Mie scattering coefficients $T_n^{E[H]}(\omega)$ correspond also to the electric-dipole and magnetic dipole components of the scattering T matrix of core-shell nanospheres and can be found to be[5,7,8,14]

$$T_n^E(\omega) = \frac{n_2\psi_n'(x_{3(2)})[\psi_n(x_2) - A_n\chi_n(x_2)] - \psi_n(x_{3(2)})[\psi_n'(x_2) - A_n\chi_n'(x_2)]}{\xi_n(x_{3(2)})[\psi_n'(x_2) - A_n\chi_n'(x_2)] - n_2\xi_n'(x_{3(2)})[\psi_n(x_2) - A_n\chi_n(x_2)]}, \tag{10a}$$

$$A_n(\omega) = \frac{n_2\psi_n(y_1)\psi_n'(x_1) - n_1\psi_n'(y_1)[\psi_n(x_1)]}{n_2\chi_n(y_1)\psi_n'(x_1) - n_1\chi_n'(y_1)[\psi_n(x_1)]}, \tag{10b}$$

$$T_n^H(\omega) = \frac{\psi_n'(x_{3(2)})[\psi_n(x_2) - B_n\chi_n(x_2)] - n_2\psi_n(x_{3(2)})[\psi_n'(x_2) - B_n\chi_n'(x_2)]}{n_2\xi_n(x_{3(2)})[\psi_n'(x_2) - B_n\chi_n'(x_2)] - \xi_n'(x_{3(2)})[\psi_n(x_2) - B_n\chi_n(x_2)]}, \tag{10c}$$

$$B_n(\omega) = \frac{n_2\psi_n(x_1)\psi_n'(y_1) - n_1\psi_n(y_1)[\psi_n'(x_1)]}{n_2\chi_n'(y_1)\psi_n(x_1) - n_1\psi_n'(x_1)[\chi_n(y_1)]}, \tag{10d}$$

where $n_1^2 = \varepsilon_1/\varepsilon_3$, $n_2^2 = \varepsilon_2/\varepsilon_3$, $y_1 = n_2 x_{3(1)} = k_0\sqrt{\varepsilon_2}r_1$. Also, in this case we can apply the MG formula to determine the effective permittivity ε_{eff} and permeability μ_{eff} of the NDLCCs given

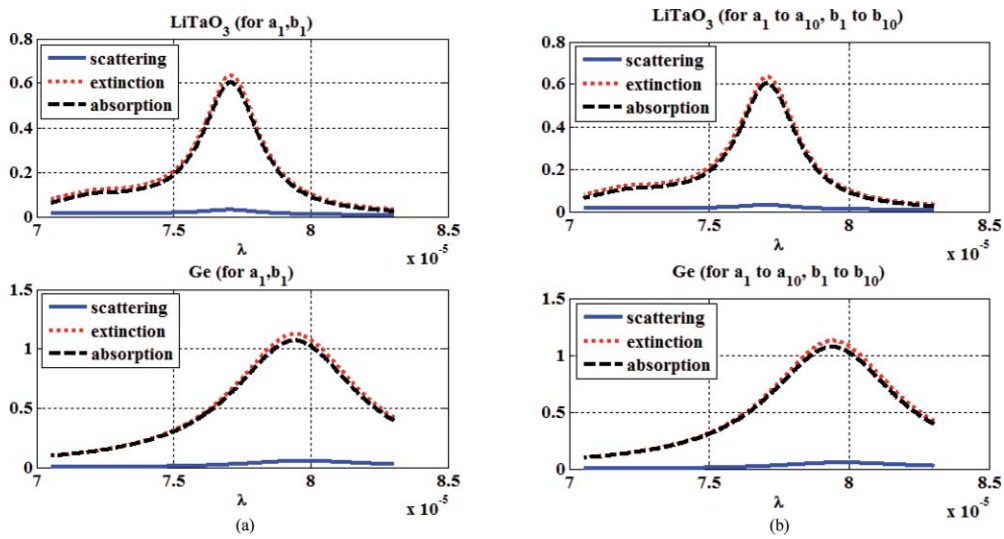

Fig. 4 Scattering, extinction, and absorption coefficients for ($LiTaO_3$, Ge), (a) for $n = 1$ and (b) for $n = 1$ to 10 terms.

by the relations

$$\varepsilon_{\text{eff}} = \varepsilon_3\left[\frac{x_{3(2)}^3 - i3fT_1^E}{x_{3(2)}^3 + i(3/2)fT_1^E}\right], \quad \mu_{\text{eff}} = \mu_3\left[\frac{x_{3(2)}^3 - i3fT_1^H}{x_{3(2)}^3 + i(3/2)fT_1^H}\right], \tag{11}$$

where f is again the volume filling fraction of the core-shell nanoparticles.

3 Numerical Method and Results

3.1 *Binary NDLCC in the FIR Regime*

Different types of nanoparticles are chosen in order to yield negative refractive index in the desired operating wavelength range. In the FIR regime, $LiTaO_3$ and Ge can be used as polaritonic and plasmonic nanoparticles, respectively.[15] Figure 4 shows the scattering, absorption, and extinction coefficients as found from Eqs. (7a)–(7c). Figure 4(a) shows the approximation using the first term ($n = 1$) only, while Fig. 4(b) uses the first 10 terms ($n = 1$ to 10). We notice that the difference is small. So, for simplicity, in finding the effective medium, we use only the first term in the remainder of the paper.

Figures 5(a) and 5(b) show n'_{eff} and n''_{eff} parts of the refractive index as a function of wavelength and the angle between the $\boldsymbol{k}$ vector of the incident light and the director axis as explained above. The following parameters were used: $r_1 = 2.8\ \mu$m, $r_2 = 2.25\ \mu$m, $\mu_1 = \mu_2 = \mu_3 = 1$, $\varepsilon_\perp = 1.96$, $\varepsilon_\parallel = 4$, $f_1 = 0.44$, $f_2 = 0.34$, $\varepsilon_0 = 15.8$, $\varepsilon_\infty = 13.4$, $\omega_p = \omega_T = 2\pi \times 4.25 \times 10^{12}$ rad/s, $\gamma_{1,2} \approx \omega_p/1000$, $\omega_L = 2 \times \pi \times 7.46 \times 10^{12}$ rad/s. We notice that the maximum negative index of refraction occurs at $\theta = 0$ which corresponds to the case when $\varepsilon_3 = \varepsilon_\perp$. Hence, we conclude that for a zero incidence angle (implying light incident normally onto the LCC), we need to apply maximum bias to the LCC in order to get the highest negative index because the majority of the LC molecules are then aligned perpendicular to the cell surface and hence parallel to the incident beam.

In order to visualize the change in the effective index of refraction throughout the NDLCC, we need to find the profile of the angle θ which affects the permittivity of the LC host. We assume that the molecules have a small (viz., 2°) pretilt in the x-z plane. The bias induced

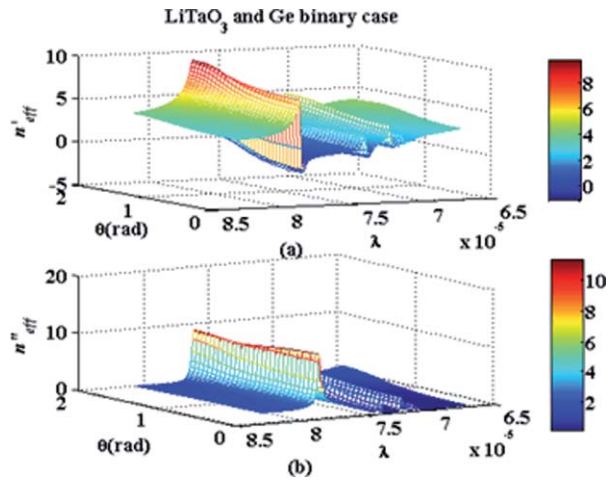

Fig. 5 Variation of (a) n'_{eff} (b) n''_{eff} with wavelength λ in the FIR and angle θ for the case of $LiTaO_3$ and Ge binary nanoparticles.

orientation is governed by the Euler–Lagrange equation:[19,20]

$$(K_1 \cos^2\theta + K_3 \sin^2\theta)\frac{d^2\theta}{dz^2} + \left(\frac{K_3 - K_1}{2}\right)\sin 2\theta\left(\frac{d\theta}{dz}\right)^2 + \frac{1}{2}\Delta\varepsilon_{st}\left(\frac{dV}{dz}\right)^2 \sin 2\theta = 0, \tag{12}$$

where θ is the angle between the molecular director and the propagation vector of the EM radiation, K_1 and K_3 are the Frank elastic constants for splay and bend, respectively, and $\Delta\varepsilon_{st} = \varepsilon_{\parallel st} - \varepsilon_{\perp st}$ is the dielectric anisotropy. The potential distribution is given by:

$$(\varepsilon_{\parallel st}\sin^2\theta + \varepsilon_{\perp st}\cos^2\theta)\frac{d^2V}{dz^2} + \Delta\varepsilon_{st}\sin 2\theta\frac{d\theta}{dz}\frac{dV}{dz} = 0. \tag{13}$$

Equations (12) and (13) are solved using a commercial software (COMSOL) which uses finite element methods with boundary conditions $V(L/2) = V_0$, $V(-L/2) = 0$, $\theta(-L/2) = \theta(L/2) = 2\pi/180$ (corresponding to 2° pre-tilt), to derive the NLC orientation across its thickness L. Typical values for E7, viz., $K_1 \approx 10$ pN, $K_3 \approx 16$ pN; $\varepsilon_{\perp st} \approx 5$, $\varepsilon_{\parallel st} \approx 20$, corresponding to a threshold voltage of approximately 0.85 V are used. This information is used to determine the permittivity profile for the host LC. This profile is thereafter discretized by decomposing the LCC into multilayers, and the effective refractive index in each layer is computed using effective medium theory. Figure 6 shows the n'_{eff} profile in the LCC due to the electric field (bias voltage) for $\lambda = 78.466$ μm which is the wavelength that gives the maximum negative effective index

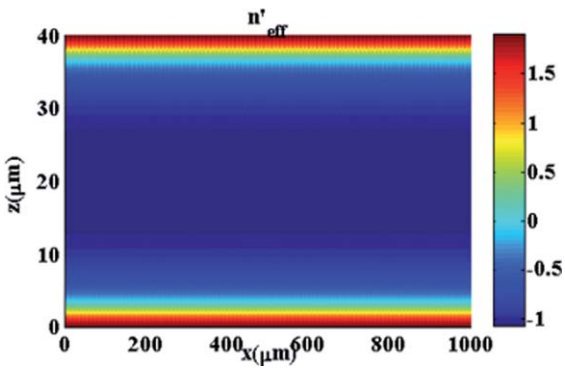

Fig. 6 n'_{eff} profile in the LCC due to bias voltage = 4V across the 40 μm cell and for λ = 78.466 μm (FIR) using $LiTaO_3$ and Ge binary nanoparticles.

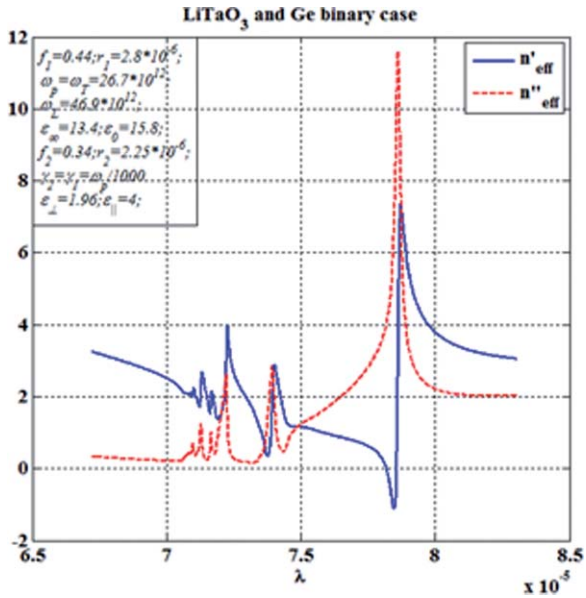

Fig. 7 n'_{eff} (solid blue) and n''_{eff} (dashed red) versus wavelength λ in FIR for normal incidence on NDLCC at high bias ($\theta \approx 0$) for the case of $LiTaO_3$ and Ge binary nanoparticles.

as shown in Fig. 5. We notice that if the bias voltage is much larger than the threshold voltage (4 V for a 40 μm sample) the bulk of the cell exhibits a negative effective index of refraction whereas at the boundaries of the cell, we may have a zero/positive index due to the anchoring effect of the LC particles with the glass slide keeping them from aligning with the electric field. For this reason the assumption of a constant θ is, indeed, valid for high values of the bias electric field. The presence of zero/positive refractive index near the boundaries of the NDLCC and negative index in the bulk of the NDLCC in this case, and other cases to follow, is in general agreement with the recent results of Pawlik et al.[21] which shows Monte-Carlo–based simulations of core-shell nanoparticles in LCs in the IR.

Figure 7 shows the real (n'_{eff}) and imaginary (n''_{eff}) parts of the effective index of refraction versus wavelength computed from Eqs. (1) to (8) and for the same parameters as before, typically in the middle of the NDLCC structure. However, for large bias as pointed out earlier, this is also a representative plot of the "average" refractive index profile as a function of wavelength, since the angle between the incident field and the director axis is predominantly $\theta \approx 0$.

To demonstrate the tunability of such a structure, we propose to vary the volume fraction of the nanoparticles inside the LCC. Figure 8 is a representative plot showing the effect on n'_{eff} of changing the volume fractions f_1 and f_2, while keeping the radii of the plasmonic and polaritonic nanoparticles at $r_1 = 4$ μm, $r_2 = 1$ μm. As a result n'_{eff} goes from negative through zero onto positive values, and the minimum achievable index over the range of variation of the volume fractions occurs when $f_1 = 0.14$, and $f_2 = 0.24$ and at approximately $\lambda = 86$ μm. Additionally, the location of the minimum depends on the volume fractions. Thus tunability of the effective index based on variations in the volume fractions of nanoparticles can be achieved.

3.2 *Binary NDLCC for the Optical Regime*

For the optical regime, one may use Au, Cu, or Ag instead of Ge as plasmonic nanoparticles since their plasma frequency is in the visible region, and use Cu_2O or CuCl instead of $LiTaO_3$ for polaritonic nanoparticles. The polaritonic material chosen for this example is CuCl due to its large exciton oscillation strength parameter (A). Similar to the FIR case discussed above, we

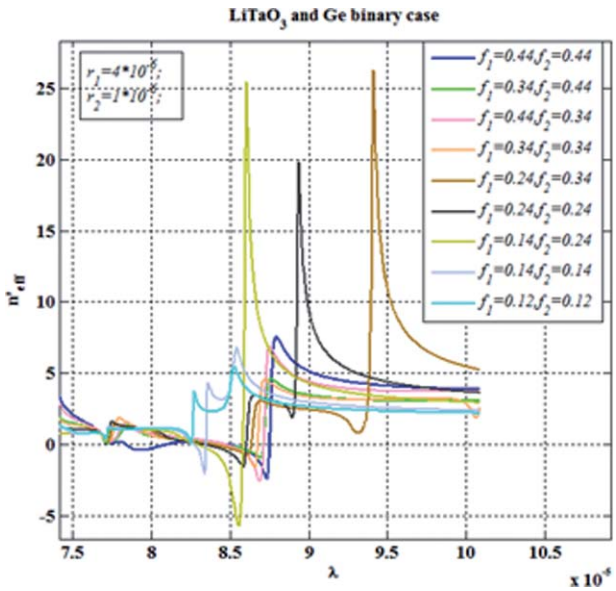

Fig. 8 The effect on n'_{eff} in FIR of changing the volume fractions f_1 and f_2, while keeping the radii of the $LiTaO_3$ and Ge binary nanoparticles unchanged.

have verified that in finding the effective medium, use of only the first term in the series in Eq. (7) is justified.

Figures 9(a) and 9(b) is the analog of Fig. 5 and show the variation of n'_{eff} and n''_{eff} as a function of wavelength in the optical regime and the angle θ between the $\boldsymbol{k}$ vector of the incident light and the director axis. The following parameters are used: $\omega_p = 2\pi \times 2.18 \times 10^{15}$ rad/s, $\omega_0 = 2\pi \times 0.775 \times 10^{15}$ rad/s, $\gamma_1 = 2\pi \times 1.2 \times 10^{10}$ rad/s, $A = 632$, $\gamma_2 = 2\pi \times 4.35 \times 10^{12}$ rad/s, $\varepsilon_\infty = 5.59$, $\varepsilon_0 = 1$, $r_1 = 35$ nm, $r_2 = 10$ nm, $\mu_1 = \mu_2 = \mu_3 = 1$, $\varepsilon_\perp = 2.3$, $\varepsilon_\parallel = 3.2$, $f_1 = 0.4$, $f_2 = 0.4$. We notice once again that the maximum negative index of refraction occurs at $\theta = 0$. As in the FIR case, the n'_{eff} profile in the NDLCC upon application of a high bias voltage (= 4V) can be calculated for the optical region (viz., at $\lambda = 0.38722$ μm). As has been plotted earlier in Fig. 6 for FIR, the results (not shown here for

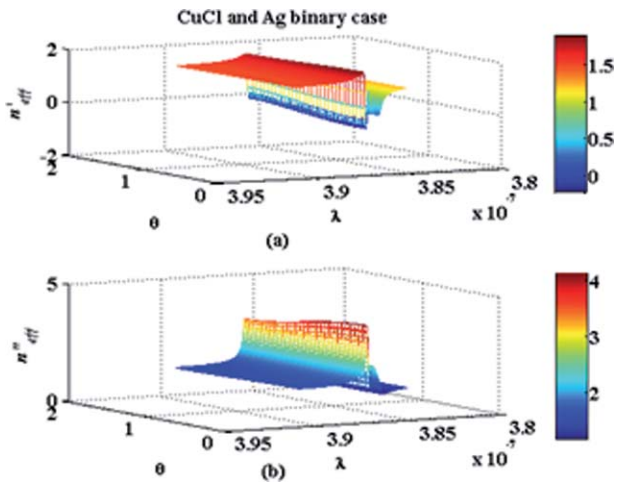

Fig. 9 (a) n'_{eff} and (b) n''_{eff} versus wavelength λ in the optical regime and angle θ for the case of CuCl and Ag binary nanoparticles.

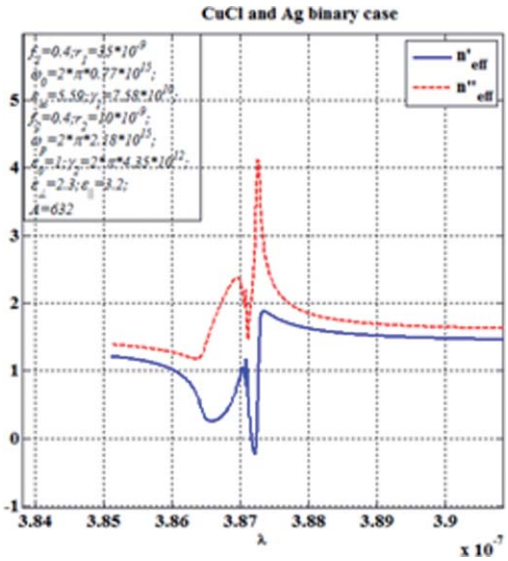

Fig. 10 n'_{eff} (solid blue) and n''_{eff} (dashed red) versus wavelength λ in the optical regime for normal incidence on NDLCC at high bias ($\theta \approx 0$) for the case of CuCl and Ag binary nanoparticles.

the sake of brevity) again show that negative index can be achieved through most of the bulk of the NDLCC, except near the boundaries.

Figure 10 shows the real (n'_{eff}) and imaginary (n''_{eff}) parts of the effective index of refraction in the optical region of the spectrum, typically in the middle of the NDLCC structure. As in the case of Fig. 7 drawn for FIR, this is also a representative plot of the average refractive index profile as a function of wavelength for large bias, since the angle between the incident field and the director axis is predominantly $\theta \approx 0$. However, in this case, tunability in the optical regime through changing the volume fractions of the nanoparticles (as shown in Fig. 11) is much less than in the FIR regime (see Fig. 8), and decreasing the volume fractions essentially result in a decrease in the magnitude of the achievable negative refractive index. The reason for this is currently under investigation, along with other methods of obtaining tunability, viz., by varying nanoparticle sizes, or preferably electronically by varying the bias voltage across the NDLCC.

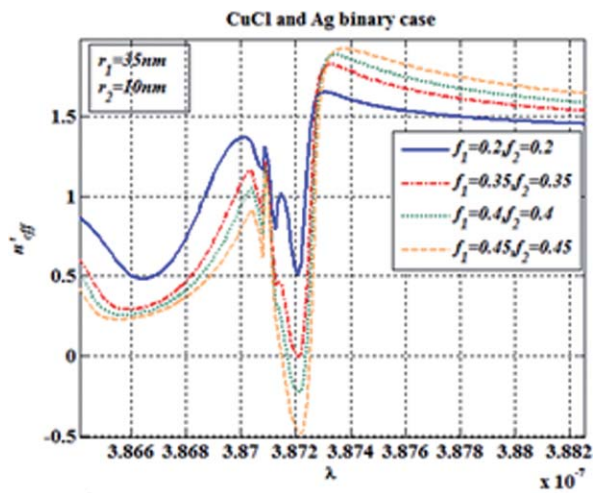

Fig. 11 The effect on n'_{eff} in the optical regime of changing the volume fractions f_1 and f_2 while keeping the radii of the CuCl and Ag binary nanoparticles unchanged.

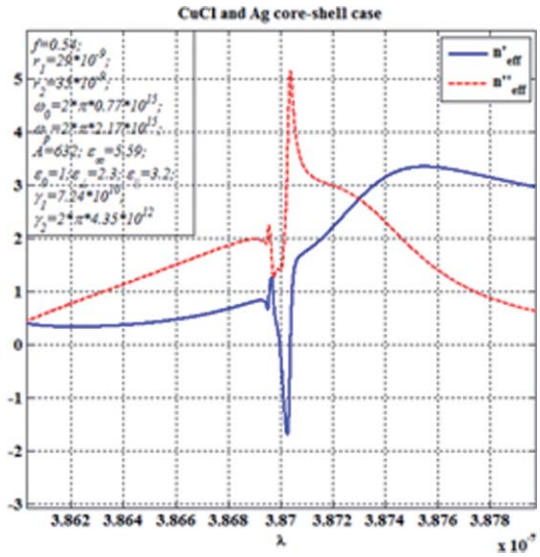

Fig. 12 n'_{eff} (solid blue) and n''_{eff} (dashed red) versus wavelength in the optical regime for normal incidence on NDLCC at high bias ($\theta \approx 0$) for the case of CuCl and Ag core-shell nanoparticles.

3.3 *Core-Shell NDLCC in the Optical Regime*

For the core-shell case in the optical regime, Fig. 12 shows the real (n'_{eff}) and imaginary (n''_{eff}) parts of the effective index of refraction computed, again for normal incidence of the light and for large bias across the NDLCC. The calculations show that for the same numerical values of r_1, r_2, which however have a different connotation than the binary case, a much larger value of negative index is achieved, although the value of n''_{eff} is somewhat larger.

Figure 13 shows the effect on n'_{eff} of keeping the same shell thickness while changing r_1, r_2. We notice that the location of the minimum peak changes as well as its value, suggesting tunability of such a device.

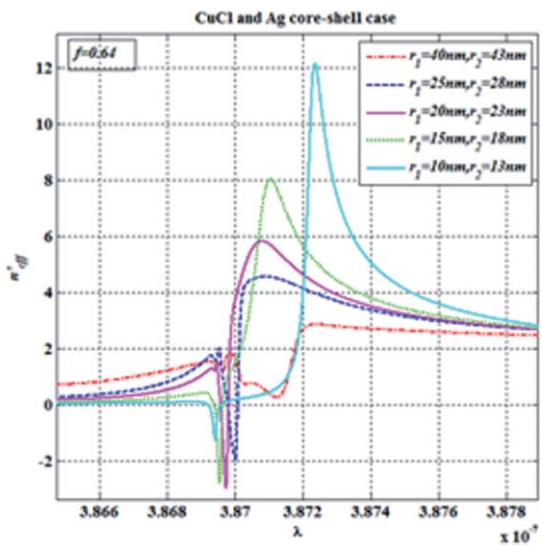

Fig. 13 Variation of n'_{eff} with wavelength in the optical regime showing the effect of keeping the same shell thickness while changing the radii of the core and the shell of the nanoparticles, $f = 0.64$.

We have also studied the effect of varying the shell thickness on the variation of n'_{eff} for the following parameters: $r_2 = 31$ nm and $r_1 = [30, 29, 28, 27, 26, 25]$ nm. We have found that the maximum negative refractive index occurs when the shell thickness is approximately 4 nm with a slight shift of the location of the minimum peak. Finally, we have studied the effect on n'_{eff} of changing the volume fraction f while keeping the radii of the core and the shell fixed at $r_1 = 29$ nm, $r_2 = 35$ nm. We find that, as expected, decreasing f results in n'_{eff} going from negative through zero to finally all positive values.

4 Conclusion

In this paper we have theoretically studied a class of possible cheap, easy to fabricate, tunable metamaterials based on NDLCCs comprising different binary nanoparticles in the IR and optical regimes, and core-shell nanoparticles different from those used in Refs. [5–8] in the optical regime, that could possibly be of great importance due to potential applications in super-resolution lensing and sensors. The effective index of refraction is calculated according to the quasistatic limit of the extended MG theory. In the process, we have also taken into account the spatial variation in the permittivity, or equivalently the refractive index, of the host LC when a bias voltage is applied to the NDLCC structure. To achieve this, we have used the intrinsic refractive index (or permittivity) profile of the liquid crystal under bias to find the effective refractive indices of each layer and hence deduce the overall refractive index of the composite binary nanoparticle dispersed nematic liquid crystal structure with bias. The tunability of these cells based on nanoparticle sizes and filling fractions has also been studied. Our calculations show that for the choices of nanoparticles described, it is indeed possible to find a negative refractive index over a range of wavelengths. For instance, using CuCl and Ag binary (as well as core-shell) nanoparticles of appropriate dimensions and filling factors, a negative index is predicted around a wavelength of 0.387 μm (visible). Similarly, using $LiTaO_3$ and Ge binary nanoparticles of appropriate dimensions and filling factors, negative index is predicted around a wavelength of 77 μm (FIR). A more rigorous analysis using optimization techniques for the volume fraction and radii of the nanoparticles needs to be done for obtaining the highest negative index in a typical cell. Electronic tunability, as well as the ability to change the overall net negative index based on net optical path length through the structure, add to the uniqueness of the design. While one of the drawbacks of these NDLCC structures is the rather high absorption, we hope that by carefully choosing and incorporating the right active materials such as dyes along with the nanoparticle mixture, transmission through these NDLCC structures in the negative index regime can be greatly enhanced.

References

1. J. B. Pendry, "Negative refraction makes a perfect lens," *Phys. Rev. Lett.* **85**, 3966–3969 (2000).
2. V. G. Veselago, "The electrodynamics of substances with simultaneously negative value of ε and μ," *Sov. Phys. Usp.* **10**, 509–514 (1968).
3. R. Aylo, P. P. Banerjee, A. K. Ghosh, and P. Verma, "Design of metamaterial based photonic sensors for pressure measurement" *Proc. SPIE.* **7604**, 760412 (2010).
4. W. Cai, "Optical cloaking with metamaterials," *Nat. Photon.* **1**, 224–227 (2007).
5. I. C. Khoo, D. H. Werner, X. Liang, A. Diaz, and B. Weiner, "Nanosphere dispersed liquid crystals for tunable negative-zero-positive index of refraction in the optical and terahertz regimes," *Opt. Lett.* **31**, 2592–2594 (2006).
6. I. C. Khoo, A. Diaz, S. Kubo, J. Liou, M. Stinger, T. Mallouk, and J. H. Park, "Nano-dispersed organic liquid and liquid crystals for all-time-scales optical switching and tunable negative- and zero- index materials," *Mol. Crys. Liq. Cryst.* **485**, 934–944 (2008).
7. J. A. Bossard, X. Liang, L. Li, Y. Seokho, D. H. Werner, B. Weiner, T. S. Mayer, P. F. Cristman, A. Diaz, and I. C. Khoo, "Tunable frequency selective surfaces and negative-

zero-positive index metamaterials based on liquid crystals," *IEEE Trans. Antennas Prop.* **56**, 1308–1320 (2008).
8. I. C. Khoo, A. Diaz, J. Liou, M. V. Stinger, J. Huang and Y. Ma, "Liquid crystal tunable optical metamaterials," *IEEE J. Sel. Topics Quantum Electron.* **16**, 410–417 (2010).
9. I. C. Khoo, Y. Williams, A. Diaz, K. Chen, J. Bossard, D. Werner, E. Graugnard, and C. J. Summers, "Liquid crystals for optical filters, switches and tunable negative index material development," *Mol. Cryst. Liq. Cryst.* **453**, 309–319 (2006).
10. R. Aylo, P. P. Banerjee, and G. Nehmetallah, "Tunable metamaterial binary nano-particle dispersed liquid crystal cells," *Proc. SPIE* **7754**, 775409 (2010).
11. R. Pratibha, K. Park, I. Smalyukh, and W. Park, "Tunable optical metamaterial based on liquid crystal-gold nanosphere composite," *Opt. Express* **17**, 19459–19469 (2009).
12. G. A. Niklasson, C. G. Grangvist, and O. Hunderi, "Effective medium models for the optical properties of inhomogeneous materials," *Appl. Opt.* **20**, 26–30 (1981).
13. C. F. Bohren and D. R Huffman, *Absorption and Scattering of Light by Small Particles*, Wiley, New York (2004).
14. M. S. Wheeler, J. S. Aitchison, and M. Mojahedi, "Three-dimensional array of dielectric spheres with an isotropic negative permeability at infrared frequencies," *Phys. Rev B* **72**, 193103 (2005).
15. V. Yannopapas, "Negative refraction in random photonic alloys of polaritonic and plasmonic microspheres," *Phys. Rev. B* **75**, 035112 (2007).
16. K. C. Huang, M. L. Povinelli, and J. D. Joannopoulos, "Negative effective permeability in polaritonic photonic crystals," *Appl. Phys. Lett* **85**, 543–545 (2004).
17. V. Yannopapas, "Artificial magnetism and negative refractive index in three-dimensional metamaterials of spherical particles at near-infrared and visible frequencies," *Appl. Phys. A* **87**, 259–264 (2007).
18. W. Park and Q. Wu, "Negative effective permeability in metal cluster photonic crystal," *Solid State Commun.* **146**, 221–227 (2008).
19. I. C. Khoo, *Liquid Crystals: Physical Properties and Nonlinear Optical Phenomena*, Wiley, New York (1995).
20. M. Peccianti, A. Fratalocchi, and G. Assanto, "Transverse dynamics of nematicons," *Opt. Express* **12**, 6524–6529 (2004).
21. G. Pawlik, M. Jarema, W. Walasik, A. C. Mitus, and I. C. Khoo, "Field-induced inhomogeneous distribution of a nanodispersed nematic liquid crystal metamaterial near the Freedericksz transition: Monte Carlo studies," *J. Opt. Soc. Am. B* **27**, 567–576 (2010).

Georges Nehmetallah received his PhD from The University of Dayton in 2006. Since then, he has published more than 37 refereed journal papers and conference proceedings, and invited book chapters and he has been working at the University of Dayton as a Research Engineer, carrying out research in digital holography, metamaterial applications to sensors technology, and nanoparticle dispersed liquid crystal cell fabrication and characterization. He is the recipient of the University of Dayton Quatman Scholarship (2003), the Newport Spectra-Physics Research Excellence Awards (2005), SPIE Educational Scholarship in Optical Science and Engineering (2005), Dayton Area Graduate Studies Institute (DAGSI) Scholarship (2004-2006).

Rola Aylo received her PhD from The University of Dayton in 2010. She has published more than 12 refereed journal papers and conference proceedings and she has been working at the University of Dayton as a Postdoctorate Researcher, carrying out research in optical design, metamaterial applications to sensors technology, and nanoparticle dispersed liquid crystal cell fabrication and characterization. She is the recipient of the University of Dayton Innovation Incentive Graduate Research Assistantships (2007), the SPIE Newport spectra research excellence award (2009), and the Dayton Area Graduate Studies Institute (DAGSI) Scholarship (2008-2009).

Partha P. Banerjee is Professor of ECE and Electro-Optics at the University of Dayton, where he was Chair from 2000-2005. Previously he was Professor of ECE at the University of Alabama in Huntsville. His areas of interest are optical processing, sensing, image processing, holography, metamaterials, acousto-optics, and photorefractives. He has authored or coauthored over 100 refereed journal publications, over 100 conference papers, four textbooks, and several invited book chapters. He has received over $4 M in funding over the last 20 years. He is Fellow of the SPIE and of the OSA, and is a senior member of the IEEE. He received the NSF Presidential Young Investigator Award in 1987.